Materials Today Communications 8 (2016) 91–99

Contents lists available at ScienceDirect

Materials Today Communications

journal homepage: www.elsevier.com/locate/mtcomm

Enthalpy-driven selective loading of $CdSe_{0.75}S_{0.25}$ nanoalloys in triblock copolymer polystyrene-*b*-polyisoprene-*b*-polystyrene

Görkem Aşkın[a], Volkan Çeçen[b], Seçil Sevim Ünlütürk[a], Serdar Özçelik[a], Mustafa M. Demir[a,c,*]

[a] İzmir Institute of Technology, Department of Chemistry, 35430 Gülbahçe, Urla, İzmir, Turkey
[b] Dokuz Eylül University, Bergama Vocational School, 35700, Bergama, İzmir, Turkey
[c] İzmir Institute of Technology, Department of Materials Science and Engineering, 35430 Gülbahçe, Urla, İzmir, Turkey

ARTICLE INFO

Article history:
Received 20 May 2016
Received in revised form 15 June 2016
Accepted 17 June 2016
Available online 18 June 2016

Keywords:
Block copolymer
Polymer nanocomposites
Quantum dots
Selective loading

ABSTRACT

$CdSe_{0.75}S_{0.25}$ nanoalloys were blended with asymmetric triblock copolymer of polystyrene-b-polyisoprene-b-polystyrene(PS-SIS) in tetrahydrofuran. The fraction of styrene block varies from 14 to 22% with respect to isoprene by mass. The morphology of the copolymer cast film experiences a phase change from cylinder to lamella. $CdSe_{0.75}S_{0.25}$ nanoalloys were prepared by two-phase method. The surface of the nanoalloys was capped by either oleic acid (OA) or *n*-tri-octylphosphonic acid (TOPO) in situ. The mean diameter of the alloyed particles is around 12 nm in both systems. The chemical nature of the nanoalloy surface was found to influence the dispersion of the particles over polymer volume. The size of the nanoalloy domains in PS is 50 nm, on average, consisting of approximately 0.7 wt% nanoalloys. However, the size of the nanoalloy domains is smaller when they are loaded into PS-SIS. The structure formation is predominantly determined by enthalpic compatibilization. Atomic force microscopy results suggest that the nanoalloys capped with TOPO sequester into PS-rich domains and enlarge the domain. On the other hand, the ones capped with OA prefer to locate in polyisoprene domains. The increase of particles over 1.0 wt% distorts the lamella structure.

1. Introduction

Block copolymers (BCPs), with their rich diversity of structures at nanometer length scales, are ideal to serve as an ordered matrix for a controlling pattern and location of particles in composite systems [1–22]. The association of particle content with BCP has attracted increased attention because the microphase separation in a block copolymer can direct the spatial distribution of nanoparticles (NP) and quantum dots (QDs), and thereby novel or improved properties can be achieved [4].

Many reviews for various aspects of BCP nanocomposites have been published [4,5,8,12,15,16,18,19,22–41]. To this end, considerable progress has been made in selectively controlling the distribution and location of QD/NP into the desired BCP domains [5,12,16,24,32,42,43]. Thermodynamic variables; i.e. entropic contributions and enthalpic differences between the surface of the particles and the polymer matrix govern the dispersion of the particulate objects in the multiphase polymer volume. Entropy of the system is defined as d/L, where d is the diameter of the particle and L is the thickness of the polymer domain [1,44]. For instance, Bockstaller et al. reported a structure formation of a ternary system consisting of poly(styrene-*b*-ethylene propylene) and small Au and large SiO_2 particle species [44] so that selective loading is achieved in long range. The particles were aliphatic coated such that the enthalpic difference between the particles and surrounding block copolymer matrix is minimized. While large particles reside in PEP domains, small Au particles locate at the interface. It was claimed that large particles reduce the conformational entropy since the number of conformations is limited for chains in the presence of the particles [44]. The conformational entropy is balanced with a translational one for the smaller particles. The same group reported enthalpic compatibilization of guest particles and surrounding block copolymer matrix depends on the topology and architecture of the polymer domain and the amount of polymeric coating present on the particle surface. The formation of both polymeric counterparts requires precise and tedious synthesis steps.

* Corresponding author at: İzmir Institute of Technology, Department of Chemistry, 35430 Gülbahçe, Urla, İzmir, Turkey.
E-mail address: mdemir@iyte.edu.tr (M.M. Demir).

http://dx.doi.org/10.1016/j.mtcomm.2016.06.004
2352-4928/

The usage of common commercial capping agents that have favorable interactions with one of the copolymer phases can simplify the assembly particles over block copolymer volume.

Previously, favorable enthalpic interactions between NP and polymer have led to order-to-order (OOT) and/or disorder-to-order phase transitions [45]. For example, hydrogen bonding of mercaptoacetic acid-coated CdSe NPs with P4VP made the polymer more stretched at the interfacial region. This change in the polymer conformation led to cylindrical-to-lamellar phase transition above 7.0 wt% of CdSe NP in the P4VP domains of PS-P4VP BCP [46]. A cylinder → distorted cylinder → disordered type order-to-disorder (ODT) phase transition was observed when the concentration of cadmium sulfide NPs in the poly(ethylene oxide) (PEO) domains of PS-PEO BCP exceeded 8.3 vol% (43 wt%) [47]. Lin et al. observed that PS-*b*-P2VP films with a hexagonal columnar morphology, with columns parallel to the substrate, changed their orientation to a hexagonal columnar morphology with columns orthogonal to the substrate upon incorporation of trioctylphosphine oxide (TOPO) covered CdSe nanoparticles [48]. Since the P2VP columns were selectively capped with the TOPO-covered nanoparticles, the authors suggested that the reorientation was driven by a lowering of the surface energy as the hydrocarbon-coated CdSe nanoparticles with a low surface energy cover the high surface energy P2VP columns, thus balancing the surface energy with the low surface energy PS matrix.

In this study, we demonstrated a simple procedure to incorporate $CdSe_{0.75}S_{0.25}$ nanoalloys into an asymmetric triblock polystyrene-*b*-polyisoprene-*b*-polystyrene (PS-SIS) and control their location within different block copolymer domains by varying the composition of ligands on the particle surfaces. $CdSe_{0.75}S_{0.25}$ nanoalloys are capped with either *n*-tri-octylphosphine oxide (TOPO) or oleic acid (OA). The size of the particles remains unchanged so that entropic contribution is minimized. This model system allows to study the effect of enthalpic compatibilization of the particles and the surrounding asymmetric PS-SIS block copolymer. These nanoalloys capped with TOPO and OA were selectively incorporated into a particular region of the microdomains in PS-SIS volume by casting from tetrahydrofuran (THF). Transmission electron microscopy (TEM) and atomic force microscopy (AFM) were employed to reveal the localization of the nanoalloys. The structure of the composite films was examined at different nanoalloy contents.

2. Experimental details

2.1. Materials

The block copolymers used to produce composites were commercially available polystyrene (PS) and polystyrene-*b*-polyisoprene-*b*-polystyrene (PS-SIS) obtained from Sigma-Aldrich Co, USA (PS-SIS 14 & 22, numbers giving the styrene content in wt%). Melt flow index values of the PS, PS-SIS 14% and PS-SIS 22% are 1.30 g/10 min, 11.0 g/10 min, and 3.0 g/10 min, respectively (200 °C/5.0 kg). The density of the block copolymers is 1.04 g/mL, 0.92 g/mL, and 0.93 g/mL at 25 °C, respectively. The molecular weight (M_w) and polydispersity index of PS are 350 kg/mol and 2.06, respectively. PS-SIS 14% has a number average molecular weight in range of 207–237 kg/mol. The molecular weight (M_w) of PS-SIS 22% is 208 kg/mol and its polydispersity index is 1.49 [49]. Tetrahydrofuran (THF), toluene, and *N*,*N*-dimethlyformamide (DMF) used as solvents were supplied by Sigma-Aldrich, USA. All of the chemicals used in this work were of the highest purity and were purchased from the Sigma-Aldrich Co. They were used without further purification.

Table 1
Composition of PS-SIS/nanoalloy particle dispersion cast to obtain composite films. The PS-SIS content of the dispersion in THF is fixed around 20 wt%. The concentration of the particles is in the range of 0.7–2.7 wt% (0.1–0.4 vol%).

Type of polymers	Styrene %	Mass % of the nanoalloy particles
PS[a]	0	0.7, 2.7
14% PS- SIS	14	–
14% PS- SIS[a]	14	0.7, 0.9, 1.3
22% PS- SIS	22	–
22% PS- SIS[a]	22	0.7, 0.9, 1.3, 2.7
22% PS- SIS[b]	22	0.7, 0.9, 1.3, 1.8, 2.7

[a] $CdSe_{0.75}S_{0.25}$/THF (capped with TOPO) dispersion was added in solvated THF PS-SIS.
[b] $CdSe_{0.75}S_{0.25}$/THF (capped with OA) dispersion was added in solvated THF PS-SIS.

2.2. Methods

2.2.1. Synthesis of $CdSe_{0.75}S_{0.25}$ nanoalloys

The ternary $CdSe_{0.75}S_{0.25}$ nanoalloys were synthesized by a modified two-phase method as introduced in a previous report [50]. While cadmium myristate (CdMA) and sodium hydrogen selenide (NaHSe) were prepared individually as Cd and Se precursors, thiourea was used as the S precursor.

In the preparation of CdMA, 10 mmol of cadmium oxide (CdO) were mixed with 20 mmol of myristic acid at 200 °C for ten minutes under vigorous stirring. When the optically clear solution was obtained, the reaction mixture was cooled, and then synthesized CdMA was recrystallized with toluene. Purified CdMA was dried at room temperature and stored as stock for the synthesis of $CdSe_{0.75}S_{0.25}$ nanoalloys.

NaHSe was synthesized by the reduction of 0.4 mmol selenium powder with 1 mmol $NaBH_4$ in 1 mL distilled water under an inert atmosphere at room temperature. When the clear solution was obtained, NaHSe was used directly by a syringe. There is no need for further purification for NaHSe solutions, but it should be freshly synthesized just before the synthesis of $CdSe_{0.75}S_{0.25}$ nanoalloys.

Tri-*n*-octylphosphine oxide (TOPO) or oleic acid (OA) was used as a capping agent for the nanoalloys. In a typical synthesis, 0.4 g CdMA and 2.0 g desired capping agent was dissolved in 80 mL toluene at 80 °C. Chalcogen precursors – the mixture of NaHSe and thiourea – and was mixed in a round bottom flask at 80 °C under vigorous stirring under inert atmosphere. The formation of ternary nanoalloys was begun when the prepared organic phase was added to the reaction flask. Sampling was done in specific time intervals in order to monitor the growth process of nanoalloys during the reaction time. Optical spectra (absorption ad photoluminescence spectra) and dynamic light scattering (DLS) measurements were used to follow the optical properties and size distribution of nanoalloys, respectively. The reaction was terminated when the desired optical properties or size distribution was obtained by cooling the reaction flask. The nanoalloys were purified by the precipitation with the addition of ethanol to the toluene solution. After centrifugation, supernatant was decanted and precipitated nanoalloys were dried at room temperature.

2.2.2. Preparation of cast-film of PS-SIS with $CdSe_{0.75}S_{0.25}$

The composite films were obtained by casting from THF. The solid content of the dispersion is around 20 wt%. The compositions of the $CdSe_{0.75}S_{0.25}$ nanoalloys and PS-SIS block copolymers used in this work are summarized in Table 1. The $CdSe_{0.75}S_{0.25}$/PS-SIS nanocomposite film specimens were prepared by solvent casting a mixture of nanoparticles and polymers in tetrahydrofuran onto a glass substrate. The films were subjected to annealing under an atmospheric condition at 25 °C for 24 h. Subsequent removal of any residual solvent was carried out under a vacuum for an additional 24 h. The thickness of the resulting films is around 50 μm.

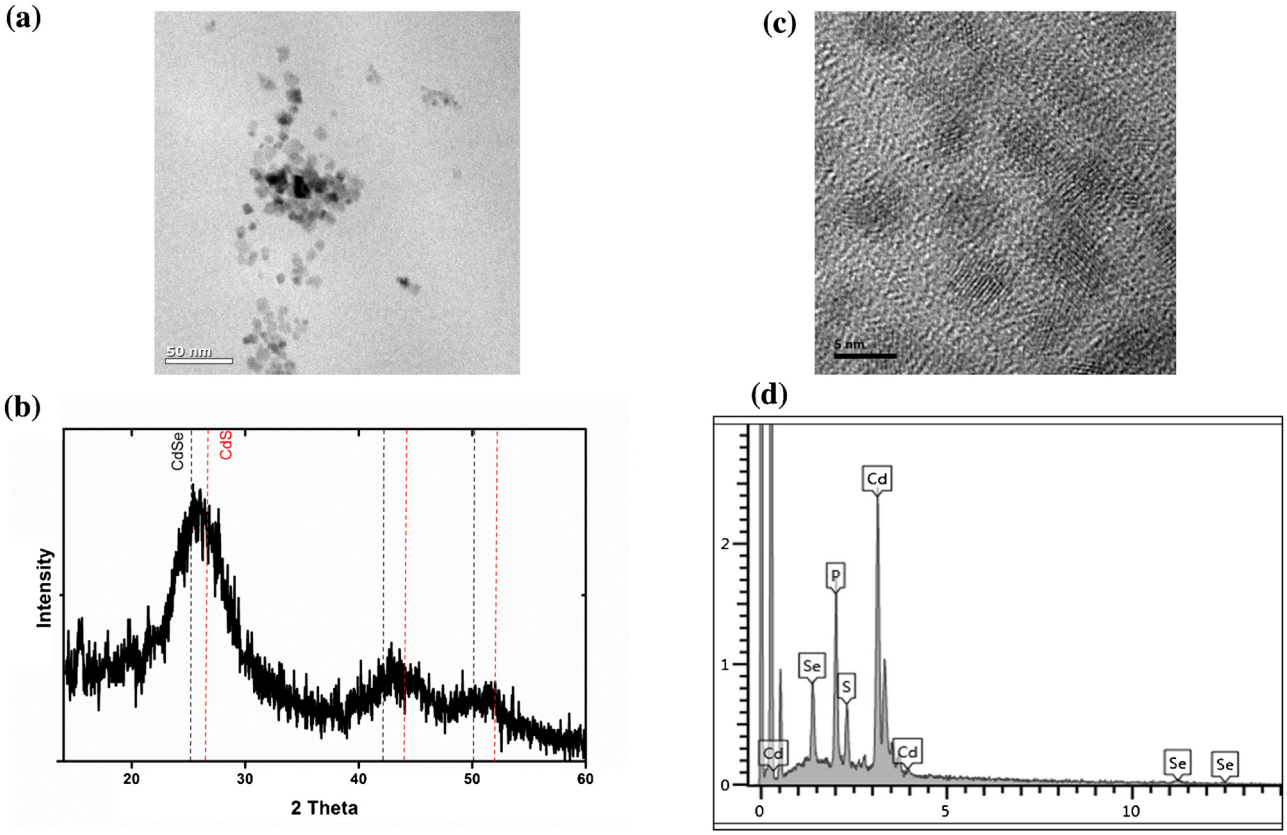

Fig. 1. (a) TEM image of TOPO-capped nanoalloys, (b) XRD of the TOPO-capped nanoalloys, (c) HRTEM of the 2.0 nm sized $CdSe_{0.75}S_{0.25}$ nanoalloys, (d) EDS spectrum of TOPO-capped nanoalloys.

2.2.3. Characterization of $CdSe_{75}S_{0.25}$ nanoalloys

Various techniques were used for the optical and compositional characterization of $CdSe_{0.75}S_{0.25}$ nanoalloys at room temperature. The purified and powdered $CdSe_{0.75}S_{0.25}$ nanoalloys were analyzed by X-ray diffraction (XRD) and scanning electron microscopy equipped with energy dispersive X-ray spectroscopy (SEM-EDS) techniques for the compositional analysis. XRD measurements were performed by Panalytical X'Pert Pro Materials Research Diffractometer with CuKa radiation (λ = 1.5406 Å). The diffractograms were matched with JCPDS card of CdS and CdSe binary type nanoparticles. The SEM-EDS analysis was carried out in Philips XL 30S FEG with an EDS detector. Malvern Zetasizer Nano ZS were used to perform the DLS measurements to obtain the size distribution of nanoalloys. A Zeiss 912 Omega microscope working at a voltage of 120 kV, or a Technai F20 microscope working at a voltage of 200 kV SFEG, was also used for the high resolution transmission electron microscope (HRTEM) and TEM-EDS analysis.

2.2.4. Characterization of composite films

Transmission electron microscopy (TEM) was carried out in a Zeiss EM 902 microscope operated at 80 kV. High-resolution TEM micrographs were obtained with a FEI Technai F20 microscope operated at 200 kV. Nanoscope IV (Digital Instruments, Tonawanda, NY, USA) was employed for AFM imaging using the tapping mode of a silicon tip.

3. Results

3.1. The synthesis and characterization of $CdSe_{0.75}S_{0.25}$

Fig. 1a depicts a representative overview TEM image of the nanoalloys. They seem spherical and uniform in size.

Fig. 1b shows a diffractogram of the alloy nanoparticles capped by TOPO. There are broad reflections (indicated with dashed lines) indexed with the crystalline structure of CdS (JCPDS no. 10-0454) and the CdSe (JCPDS no. 19-0191). The reflections are broad, indicating that the crystals are nanometer sized. Using the application of the Vegard's law, the stoichiometry of the coefficients are Se:3 and S:1, meaning that the molecular formula is $CdSe_{0.75}S_{0.25}$. Fig. 1c presents high resolution TEM images of the alloy particles. Lattice fringes of the particles that refer to the atomic planes are evident. The elemental composition of the alloy particles was determined by Energy Dispersive X-ray spectroscopy. Not surprisingly, Cd, Se, and S atoms are present in the spectrum (Fig. 1d). In addition, there is a strong P signal in the spectrum. The origin of this element should be the TOPO molecules immobilized to the surface of the $CdSe_{0.75}S_{0.25}$ particles.

Fig. 2 presents number size distribution of the TOPO- and OA-capped $CdSe_{0.75}S_{0.25}$ nanoalloys in THF dispersion. While the microscopy image covers approximately 0.01 μm^2, which consists of a limited number of nanoalloys. The scattering technique provides information from the entire population of the nanoalloys. Both systems show narrow-sized distributions with a mean diameter of around 12 nm and 13 nm, respectively. The tail of both distributions extends to 20 nm. Based on both microscopy and scattering techniques, one can conclude that the nanoalloys have uniform size and individual particle dispersion.

3.1.1. Phase separation in PS-SIS

Fig. 3 displays tapping mode AFM phase images of PS and PS-SIS containing various styrene fraction. Fig. 3a presents a composite film prepared by parent polystyrene. The surface provides low surface roughness without any surface features. However, PS is a glass and PI is rubbery at room temperature [48]. Fig. 3b displays *cylin-*

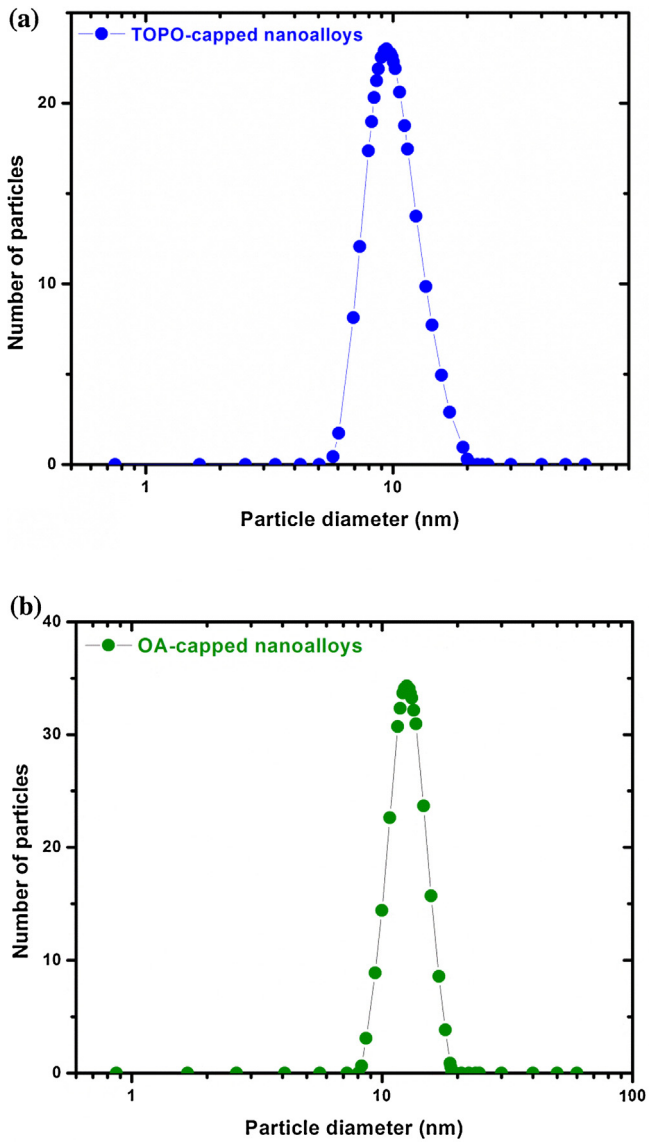

Fig. 2. DLS number size distribution of the nanoalloys capped with (a) TOPO and (b) OA.

Table 2
Domain sizes PS and PI phases in pristine PS-SIS block copolymer and nanoalloys/PS-SIS composite films.

22% PS-SIS	PS (nm)	PI (nm)
Pristine polymer	27	35
TOPO-capped $CdSe_{0.75}S_{0.25}$ nanoalloys	39	31
OA-capped $CdSe_{0.75}S_{0.25}$ nanoalloys	23	46

drical type phase separation of the copolymer consisting of 14% styrene. The round-shape dark phase represents cross sections of the cylindrical PI phases, which are perpendicularly arranged to the glass substrate. On the other hand, the light regions represent the continuous PS-rich phase.

When the fraction of PS content increases to 22%, the morphology of the phase separation changes to *lamella*. Fig. 3c presents enough contrast to observe the domains and domain spacing of the lamellar morphology. Section analysis was employed to measure the variation of the lamellar spacing. The size of lamellar domain of the PS and PI were found to be ~27 nm and ~35 nm, respectively, for the f_{PS} = 0.22 in PS-SIS (Table 2). The formation of self-assembled structures is driven by the microphase separation of different blocks of PS-SIS competing with the chemical linking between them. The findings observed here are consistent with those of the previous studies that have examined the effect of the volume ratio f_{PS} of the block copolymers on a variety of copolymer morphologies [25,51–56].

3.1.2. Effect of capping agent on phase behavior of PS-SIS

The surface of nanoalloys was treated with a capping agent, either TOPO or OA. The nanoalloys were blended with polymer solution. Fig. 4a shows tapping mode AFM images of the composite prepared by the homopolymer (PS). The bright spherical regions refer to the domains of nanoalloys. The size of the domains is nearly 50 nm. Considering that the mean diameter of nanoalloys is around 12–13 nm, the domains consist of approximately 20–30 individual particles in an aggregated state. When the alloys were mixed with PS-SIS solution f_{PS} = 0.22 as a matrix, they have four choices for location: (i) PS-rich phases, (ii) PI-rich phases, (iii) at the interphase of the two phases, and (iv) random dispersion of the nanoalloys.

The chemical nature of ligands directly influences the $CdSe_{0.75}S_{0.25}$ distribution in PS-SIS matrice. In the presence of TOPO-capped $CdSe_{0.75}S_{0.25}$ nanoalloys (0.7 wt%), the light-colored zone in the AFM image represents the PS (Fig. 4b). The small dark nanoalloys in this case are segregated selectively in PS domains. In contrast to the composite prepared by the homopolymer of styrene, the formation of large aggregates/agglomerates has not been observed. On the other hand, when the nanoalloys are capped by OA, they prefer to be located in PI-rich phases (Fig. 4c).

Although the contrast in the AFM image of the PS-SIS 22% in Fig. 5 is weak as compared to ones for the PS-SIS/$CdSe_{0.75}S_{0.25}$ nanocomposites, clearly two lamellar morphologies with different domain spacings are observed. Apparently, the sinusoidal regularity of the domains is observed in the pristine copolymer. However, the regularity is distorted upon incorporation of the nanoalloy particles into the block copolymer system. Moreover, the width of the domain spacing in the PI phase profile expands. This is because a fixed 0.75 μm length occupies 12 and 10 lamellae on average on the pristine and the composite films surface, respectively. The sections of the pristine film seem to contain more layers. The smaller number of layers observed in sections of the composite film could be attributed to the swelling of the domains by the quantum sized alloy particles. The domain spacing of the lamellar structure formed by the PI phases observed in the profiles are found to be around 35 and 46 nm for pristine and composite, respectively, as indicated in Table 2.

The domain preference of $CdSe_{0.75}S_{0.25}$ nanoalloys in PS-SIS was also validated by TEM. Fig. 6a and b show TEM images of TOPO-capped nanoalloys dispersed in a f_{PS} = 0.22 PS-SIS lamellar block copolymer phase. Enough contrast could be obtained in order to clearly observe the formed lamellar morphology of the PS and PI domains without the use of a staining agent. In these images, the dark regions correspond to the PI-rich domains; on the other hand, PS-rich domains appear as light gray. The $CdSe_{0.75}S_{0.25}$ nanoalloys, which are evident as small, darker points, are located within the PS block phase of the lamellae structure. The segregation behavior of the nanoalloys in the PS region of block copolymers can also be determined by high-resolution annular dark field imaging using a scanning transmission electron microscope (STEM) (Fig. 6b). The results indicate that $CdSe_{0.75}S_{0.25}$ nanoalloys, appearing as light points in dark field images, are found within the PS block while PI domains are almost free of particles.

The particle concentration has also been found to be an important parameter in the course of composite formation. Fig. 7 illustrates the morphological transformations for the f_{PS} = 0.22 PS-SIS block copolymers at the various OA-capped $CdSe_{0.75}S_{0.25}$ contents and represents the changes of the characteristic distribution of the nanoalloys. The lamellar morphology

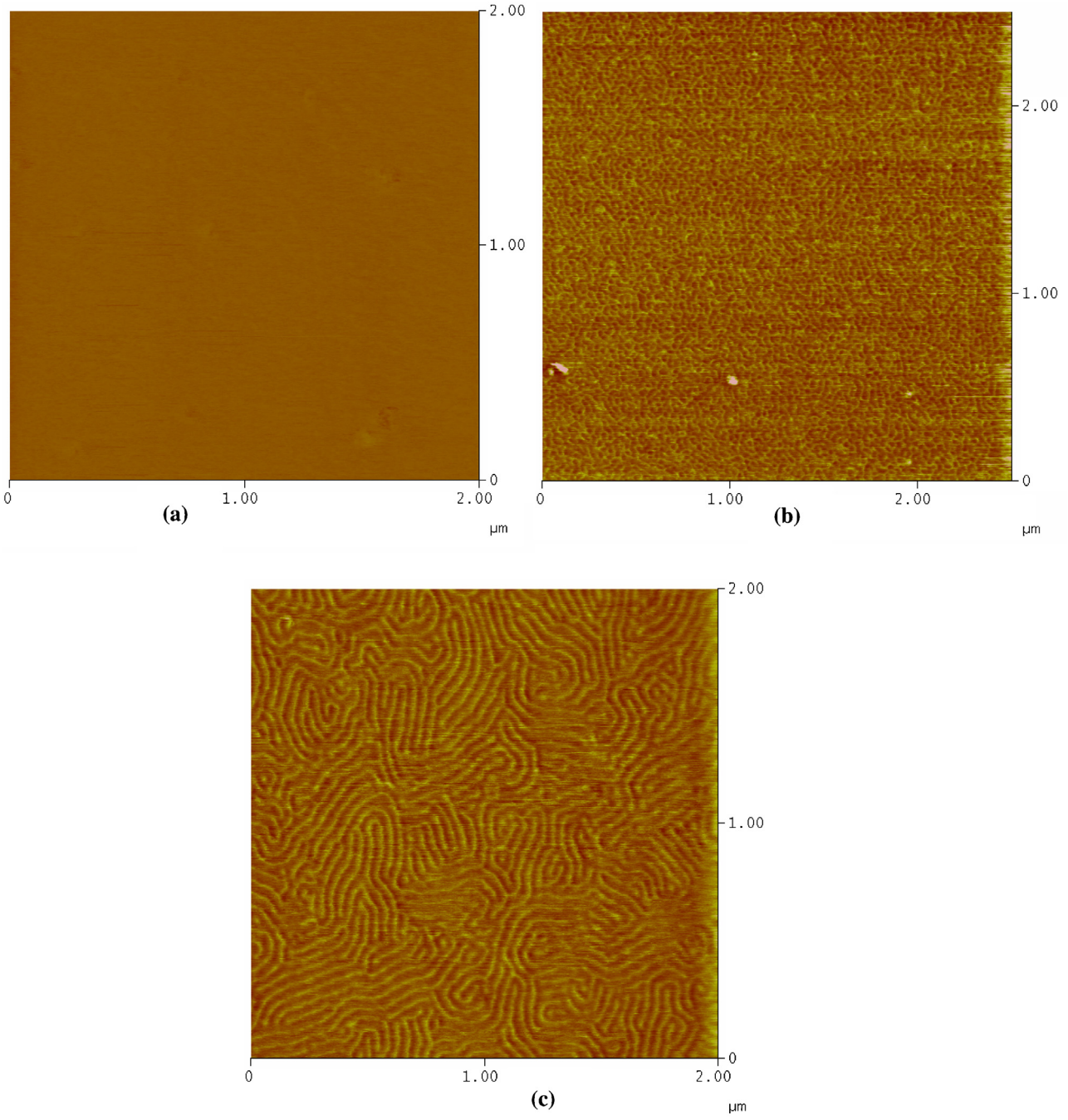

Fig. 3. Tapping mode AFM phase images of (a) PS, (b) PS-SIS, with 14% PS (c) PS-SIS with 22% PS.

of the nanocomposites is distorted when the concentration of $CdSe_{0.75}S_{0.25}$ nanoalloys in the PI block is increased (Fig. 7b and c). As the particle concentration increases, the loss of polymer conformational entropy also increases, and dispersion of the alloyed particles within the PI domain becomes increasingly unfavorable as the PI chains stretch, accommodating more particles. This can prevent a uniform distribution of $CdSe_{0.75}S_{0.25}$ throughout the PI domain. Further increases in the amount of $CdSe_{0.75}S_{0.25}$ lead to order-to-order phase transition. In the presence of 2.7 wt% the nanoalloys, as indicated in Fig. 7d, loss of polymer conformational entropy due to a larger stretching penalty could be minimized by locating more particles in the interior of the PI domains. The translational entropy of particles cannot offset the increase in the penalty of stretching, and thus OA-capped $CdSe_{0.75}S_{0.25}$ nanoalloys are prevented from spreading throughout the PI domains. A similar trend is also observed for the PS-SIS containing $f_{PS} = 0.14$ of PI segments at higher nanoalloys content.

4. Discussion

The successful navigation of nanoparticles (NPs) in a particular location of the block copolymer matrix and conferral of functional properties are governed by various enthalpic and entropic contributions to the total free energy [41]. This is the result of a balance between the polymer conformational entropy, NP translational entropy, and enthalpy of NP insertion caused by the creation of polymer-NP interfaces [41,57–60]. The overall change in free energy resulting from the total change in enthalpy and entropy of

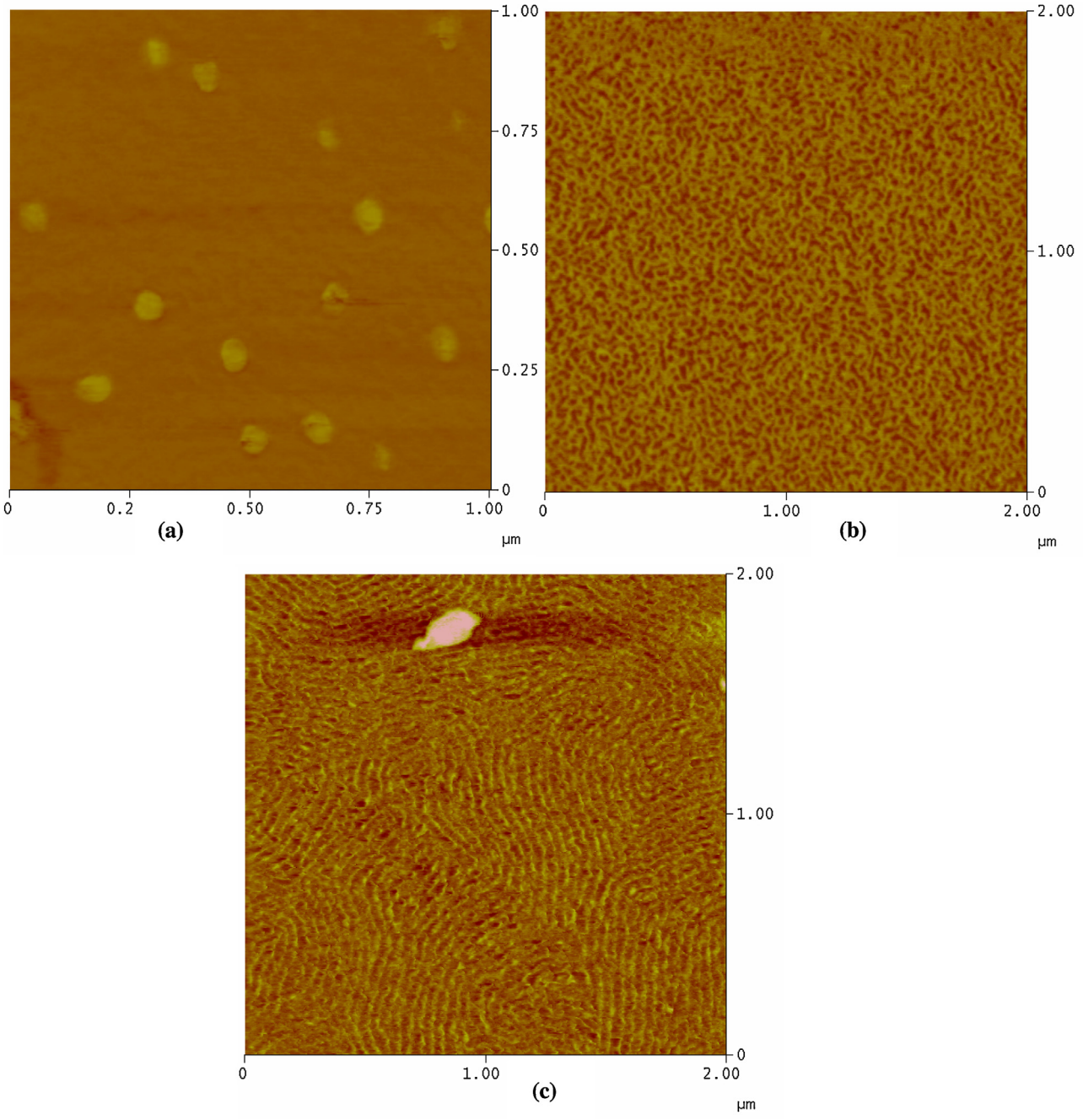

Fig. 4. Tapping mode AFM phase images of composites containing 0.7 wt% nanoalloys. (a) PS consisting of TOPO-capped nanoalloys, (b) PS-SIS with 14% PS consisting of TOPO-capped nanoalloys (c) PS-SIS with 22% PS consisting of OA-capped nanoalloys.

the composite systems plays a critical role of NP dispersion in BCP volume and the overall morphology of the resulting composites [41,61,62]. Depending on the nature of polymer/particle interactions, particles can be located selectively at the interior of the domains formed by a particular block or localized at the interface, where different polymer blocks join [61].

Rather than the copolymer consisting of 14% styrene, the current discussion deals with the domain selectivity of the $CdSe_{0.75}S_{0.25}$ nanoalloys into the PS-SIS consisting of 22% styerene since their AFM images support the assertions concerning the localization of nanoalloys through the respective polymer domain. For $f_{PS} = 0.22$, OA-capped $CdSe_{0.75}S_{0.25}$ nanoalloys were confined selectively to the PI block (Fig. 4c). This selective loading could be attributed to the minimization of the conformational entropy loss for the PI block chains involved during the incorporation of the nanoalloys. A gain in enthalpy of OA-capped $CdSe_{0.75}S_{0.25}$ insertion due to the creation of PI-nanoalloy interfaces dominates over the loss in polymer conformational entropy in order to sequester OA-capped nanoalloys in the interior domains formed by the selective PI block. On the other hand, favorable enthalpic interactions originated from the contact of TOPO on the $CdSe_{0.75}S_{0.25}$ particle surface with PS domain as well as the minimum loss in polymer conformational entropy favor selective incorporation of TOPO-capped $CdSe_{0.75}S_{0.25}$ nanoalloys in the PS rich domains of the PI-PS lamellar structure (Fig. 6).

The concentration of NPs incorporated in ordered block copolymer matrices can influence the entire thermodynamic parameters mentioned above. The higher loadings of OA-capped the nanoalloys in the PI domains of lamellar structures formed was not

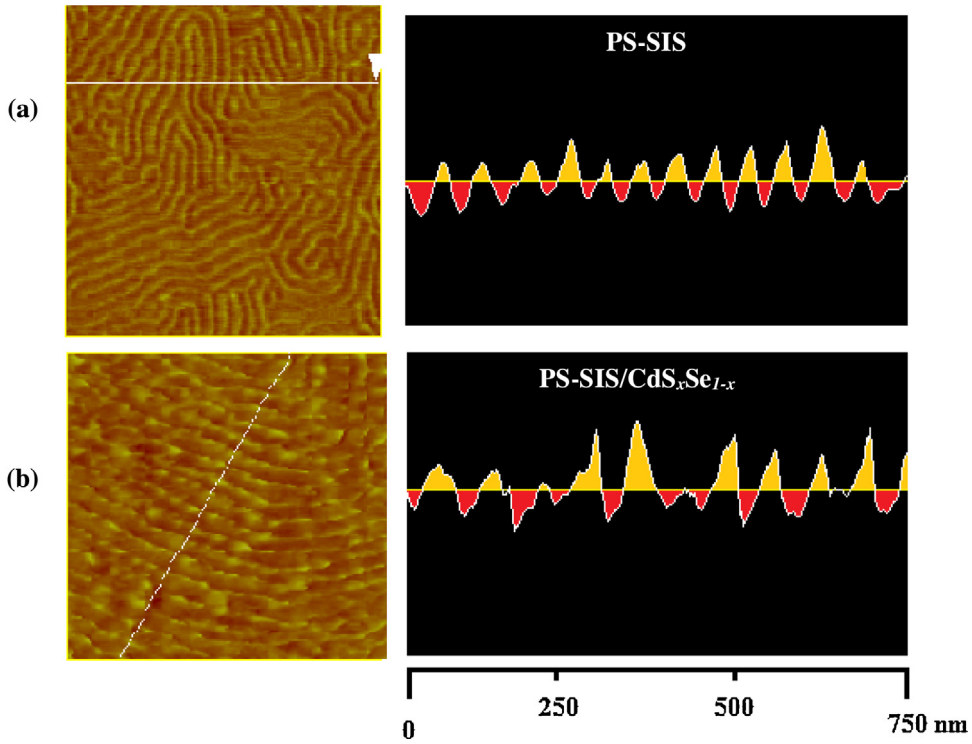

Fig. 5. Tapping mode AFM phase images of (a) PS-SIS with 22% PS, and (b) 22% PS-SIS samples containing 0.9 wt% the nanoalloys capped with OA. The red lamellae in the enlarged section of the AFM image correspond to PI domains. The white lines show the position at which the profiles illustrated on the right are created. (For interpretation of the references to colour in this figure legend, the reader is referred to the web version of this article.)

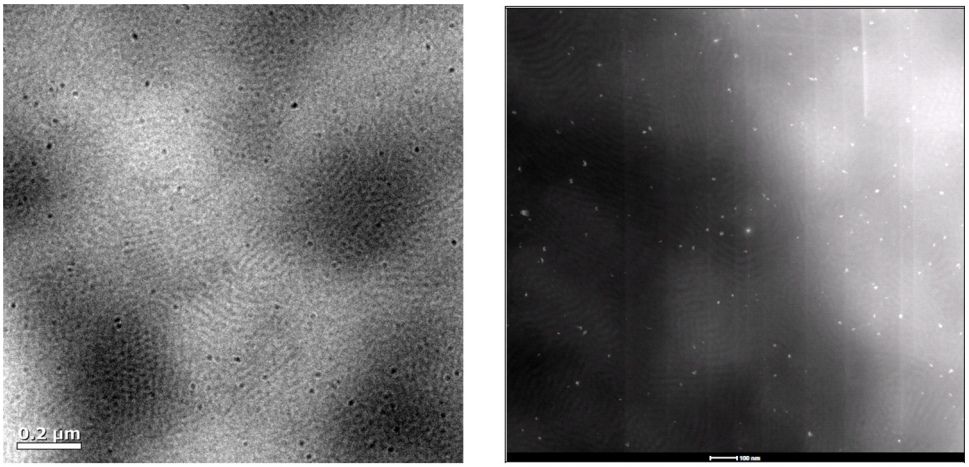

Fig. 6. Cross-sectional TEM images of an unstained sample of the 22% PS-SIS containing 0.7 wt% TOPO-capped nanoalloys. (a) bright (b) dark field (the scale bar represents 100 nm).

thermodynamically favorable since the nanoalloys incorporation was associated with a significant loss of polymer conformational entropy. This loss could not be compensated by a gain in enthalpy from favorable particle–polymer interactions. As a result, the OA-capped nanoalloys formed aggregates inside the interior of the PI domains. The entropic penalty associated with chain stretching around aggregates can give rise to order-to-disorder phase transitions. Notably, for lower nanoalloys loading, this behavior was not observed. This is because the PI domains can easily accommodate the nanoalloys without a substantial entropic penalty. Positioning the alloy near the center of the PI domain leads to a better embedding of the nanoalloys since the PI chains can accommodate alloys by moving apart rather than by stretching. The dispersion of the nanoalloys in the PI block was favored by an increased particle translational entropy.

On the other hand, $CdSe_{0.75}S_{0.25}$-rich PI domains started to precipitate out in the 1.3 wt% $CdSe_{0.75}S_{0.25}$ sample and form a trapped intermediate state in the system. At a high OA-capped $CdSe_{0.75}S_{0.25}$ nanoalloys concentration (1.8 wt% with respect to PS-SIS), the $CdSe_{0.75}S_{0.25}$/PI lamellar domains of the PS-SIS block copolymers were destroyed because of an entropic gain, mainly due to a reduced need of polymer stretching to fill the interstitial regions. It resulted in a larger polydispersity in the lamellar spacing. As a result, incorporation of OA-capped nanoalloys in PI domains led to a lamellae-to-disorder transition.

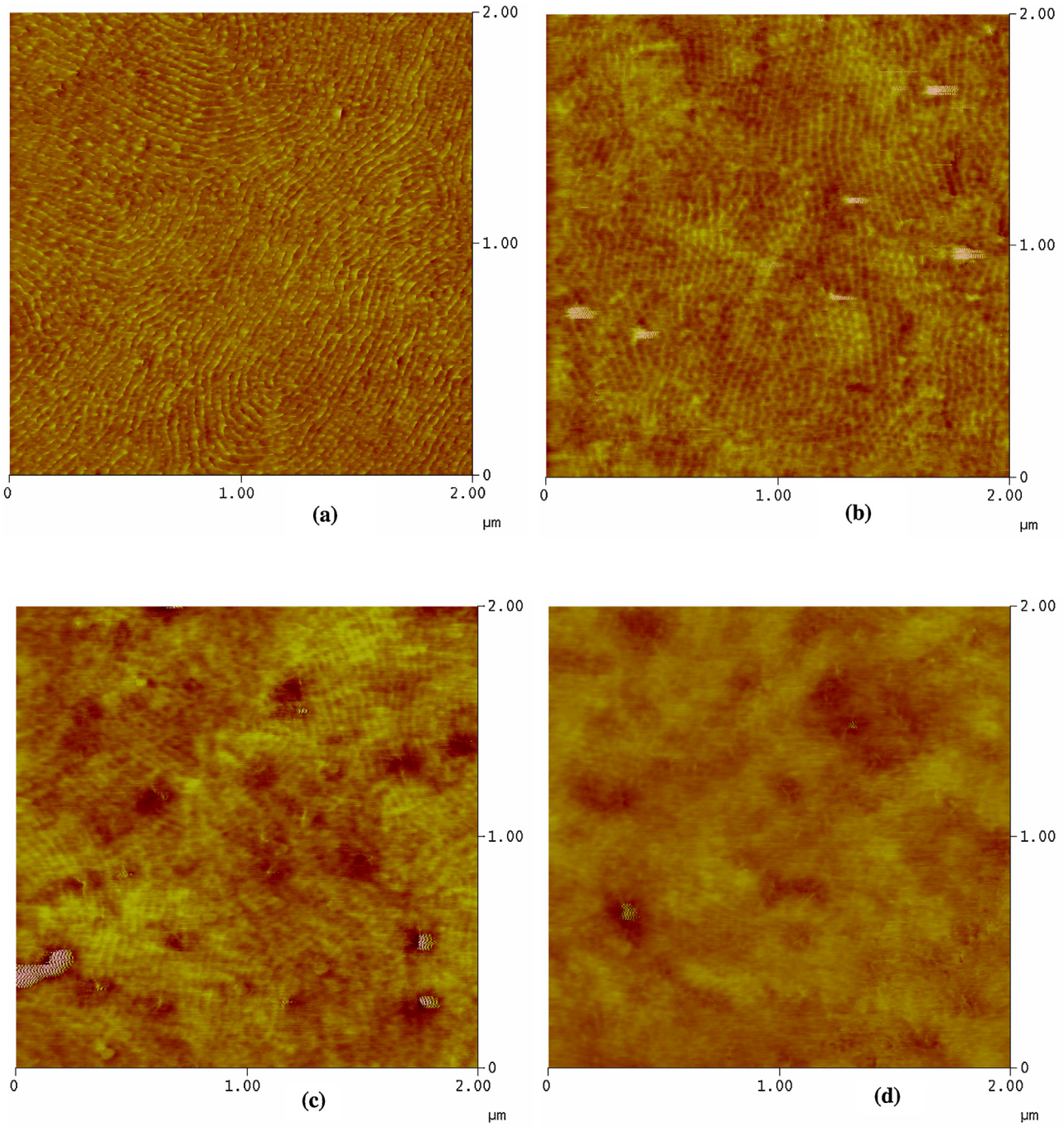

Fig. 7. Phase contrast atomic force microscopy images of 22% PS-SIS samples containing (a) 0.9, (b) 1.3, (c) 1.8 and (d) 2.7 wt% the nanoalloys capped with OA. The concentration of the particles in terms of volume percent is 0.1, 0.2, 0.3, and 0.4, respectively.

5. Conclusion

We demonstrated preferential sequestration of $CdSe_{0.75}S_{0.25}$ nanoalloys into an asymmetric triblock copolymer of polystyrene-*b*-polyisoprene-*b*-polystyrene. The alloys were treated with common commercial capping agents: *n*-tri-octylphosphine oxide or oleic acid. The surface capping/treatment leads to uniform and individual particle dispersion in THF. The alloys were blended with PS-SIS consisting of 14 or 22% styrene and film-cast from the solution. TOPO-capped $CdSe_{0.75}S_{0.25}$ nanoalloys swell selectively in the PS-rich domains from 27 to 39 nm; simultaneously, PI-rich domains shrink 35–31 nm. On the other hand, the ones capped with OA preferentially sequester to PI-rich domains. Similarly, the thickness of this domain swells; the PS-rich domains were reduced from 27 to 23. As a result, the chemistry of the ligands was found to be an important parameter for particle location as well as domain spacing. The enthalpic compatibilization governs the internal structure of the resulting photonic composites. Moreover, increasing $CdSe_{0.75}S_{0.25}$ nanoalloys content causes a phase transition from lamellae to distorted lamella. The domains intervene significantly with the lamellar structure and deteriorate substantially in the long-range order because of an entropic gain due mainly to reduced need of polymer stretching to fill the interstitial regions. This method appears to be well suited to obtain composite material for the control of particle location and it can be extended to other block copolymer and particle systems indepen-

dent of the chemistry of polymer and the particulate nanoalloys. The structure-property correlations of such composite materials is still not completely adequate, and merits further research.

Acknowledgments

The authors thank the Centre for Materials Research of Izmir Institute of Technology (IzTech) and I. Lieberwirth of Max Planck Institute for microscopy work. MMD acknowledges the “Outstanding Young Investigator” grant from Turkish Academy of Sciences (TÜBA-GEBİP 2013).

References

[1] R.B. Thompson, et al., Predicting the mesophases of copolymer-nanoparticle composites, Science 292 (5526) (2001) 2469–2472.
[2] J.Y. Lee, et al., Effect of nanoscopic particles on the mesophase structure of diblock copolymers, Macromolecules 35 (13) (2002) 4855–4858.
[3] R.B. Thompson, et al., Block copolymer-directed assembly of nanoparticles: forming mesoscopically ordered hybrid materials, Macromolecules 35 (3) (2002) 1060–1071.
[4] A.C. Balazs, T. Emrick, T.P. Russell, Nanoparticle polymer composites: where two small worlds meet, Science 314 (5802) (2006) 1107–1110.
[5] M.R. Bockstaller, R.A. Mickiewicz, E.L. Thomas, Block copolymer nanocomposites: perspectives for tailored functional materials, Adv. Mater. 17 (11) (2005) 1331–1350.
[6] W. Caseri, Nanocomposites of polymers and metals or semiconductors: historical background and optical properties, Macromol. Rapid Commun. 21 (11) (2000) 705–722.
[7] J. Ciebien, et al., Brief review of metal nanoclusters in block copolymer films, New J. Chem. 22 (7) (1998) 685–691.
[8] A.C. Balazs, Modeling self-assembly and phase behavior in complex mixtures, Annu. Rev. Phys. Chem. 58 (2007) 211–233.
[9] G. Cao, D. Liu, Template-based synthesis of nanorod, nanowire, and nanotube arrays, Adv. Colloid Interface Sci. 136 (1) (2008) 45–64.
[10] V. Castelvetro, C. De Vita, Nanostructured hybrid materials from aqueous polymer dispersions, Adv. Colloid Interface Sci. 108 (2004) 167–185.
[11] R. Cohen, Block copolymers as templates for functional materials, Curr. Opin. Solid State Mater. Sci. 4 (6) (1999) 587–590.
[12] S. Darling, Directing the self-assembly of block copolymers, Prog. Polym. Sci. 32 (10) (2007) 1152–1204.
[13] S. Förster, M. Antonietti, Amphiphilic block copolymers in structure–controlled nanomaterial hybrids, Adv. Mater. 10 (3) (1998) 195–217.
[14] R.B. Grubbs, Hybrid metal–polymer composites from functional block copolymers, J. Polym. Sci. A: Polym. Chem. 43 (19) (2005) 4323–4336.
[15] I. Hamley, Nanostructure fabrication using block copolymers, Nanotechnology 14 (10) (2003) R39.
[16] A. Haryono, W.H. Binder, Controlled arrangement of nanoparticle arrays in block-copolymer domains, Small 2 (5) (2006) 600–611.
[17] J. Hulteen, A general template-based method for the preparation of nanomaterials, J. Mater. Chem. 7 (7) (1997) 1075–1087.
[18] M. Lazzari, M.A. López-Quintela, Block copolymers as a tool for nanomaterial fabrication, Adv. Mater. 15 (19) (2003) 1583–1594.
[19] Y. Matsushita, Creation of hierarchically ordered nanophase structures in block polymers having various competing interactions, Macromolecules 40 (4) (2007) 771–776.
[20] A.B. Mayer, Colloidal metal nanoparticles dispersed in amphiphilic polymers, Polym. Adv. Technol. 12 (1–2) (2001) 96–106.
[21] C. Park, J. Yoon, E.L. Thomas, Enabling nanotechnology with self assembled block copolymer patterns, Polymer 44 (22) (2003) 6725–6760.
[22] T. Smart, et al., Block copolymer nanostructures, Nano Today 3 (3) (2008) 38–46.
[23] L.S. Schadler, et al., Designed interfaces in polymer nanocomposites: a fundamental viewpoint, MRS Bull. 32 (04) (2007) 335–340.
[24] R.A. Vaia, J.F. Maguire, Polymer nanocomposites with prescribed morphology: going beyond nanoparticle-filled polymers, Chem. Mater. 19 (11) (2007) 2736–2751.
[25] S. Förster, T. Plantenberg, From self–organizing polymers to nanohybrid and biomaterials, Angew. Chem. Int. Ed. 41 (5) (2002) 688–714.
[26] Y. Ji, J.E. Marshall, E.M. Terentjev, Nanoparticle-liquid crystalline elastomer composites, Polymers 4 (1) (2012) 316–340.
[27] C.-W. Chiu, J.-J. Lin, Self-assembly behavior of polymer-assisted clays, Prog. Polym. Sci. 37 (3) (2012) 406–444.
[28] A. Biswas, et al., Advances in top–down and bottom–up surface nanofabrication: techniques, applications & future prospects, Adv. Colloid Interface Sci. 170 (1) (2012) 2–27.
[29] L. Hsu, C. Weder, S.J. Rowan, Stimuli-responsive: mechanically-adaptive polymer nanocomposites, J. Mater. Chem. 21 (9) (2011) 2812–2822.
[30] A. Thomas, Functional materials: from hard to soft porous frameworks, Angew. Chem. Int. Ed. 49 (45) (2010) 8328–8344.
[31] M.S. Shoichet, Polymer scaffolds for biomaterials applications, Macromolecules 43 (2) (2009) 581–591.
[32] S.K. Kumar, R. Krishnamoorti, Nanocomposites: structure, phase behavior, and properties, Ann. Rev. Chem. Biomol. Eng. 1 (2010) 37–58.
[33] T. Hanemann, D.V. Szabó, Polymer-nanoparticle composites: from synthesis to modern applications, Materials 3 (6) (2010) 3468–3517.
[34] V. Ganesan, C.J. Ellison, V. Pryamitsyn, Mean-field models of structure and dispersion of polymer-nanoparticle mixtures, Soft Matter 6 (17) (2010) 4010–4025.
[35] J. Pyun, Nanocomposite materials from functional polymers and magnetic colloids, Polym. Rev. 47 (2) (2007) 231–263.
[36] A.J. Crosby, J.Y. Lee, Polymer nanocomposites: the nano effect on mechanical properties, Polym. Rev. 47 (2) (2007) 217–229.
[37] K.M. Langner, G. Sevink, Mesoscale modeling of block copolymer nanocomposites, Soft Matter 8 (19) (2012) 5102–5118.
[38] L.-T. Yan, X.-M. Xie, Computational modeling and simulation of nanoparticle self-assembly in polymeric systems: structures, properties and external field effects, Prog. Polym. Sci. 38 (2) (2013) 369–405.
[39] F.H. Schacher, P.A. Rupar, I. Manners, Functional block copolymers: nanostructured materials with emerging applications, Angew. Chem. Int. Ed. 51 (32) (2012) 7898–7921.
[40] T.N. Hoheisel, K. Hur, U.B. Wiesner, Block copolymer-nanoparticle hybrid self-assembly, Prog. Polym. Sci. 40 (2015) 3–32.
[41] B. Sarkar, P. Alexandridis, Block copolymer–nanoparticle composites: structure, functional properties, and processing, Prog. Polym. Sci. 40 (2015) 33–62.
[42] R. Shenhar, T.B. Norsten, V.M. Rotello, Polymer-mediated nanoparticle assembly: structural control and applications, Adv. Mater. 17 (6) (2005) 657–669.
[43] J. Kao, et al., Toward functional nanocomposites: taking the best of nanoparticles, polymers, and small molecules, Chem. Soc. Rev. 42 (7) (2013) 2654–2678.
[44] M.R. Bockstaller, et al., Size-selective organization of enthalpic compatibilized nanocrystals in ternary block copolymer/particle mixtures, J. Am. Chem. Soc. 125 (18) (2003) 5276–5277.
[45] C.H. Lee, et al., Ordering behavior of layered silicate nanocomposites with a cylindrical triblock copolymer, Macromol. Chem. Phys. 207 (4) (2006) 444–455.
[46] S.-W. Yeh, et al., CdS nanoparticles induce a morphological transformation of poly (styrene-*b*-4-vinylpyridine) from hexagonally packed cylinders to a lamellar structure, Macromolecules 38 (15) (2005) 6559–6565.
[47] S.W. Yeh, et al., Effect of incorporated CdS nanoparticles on the crystallinity and morphology of poly (styrene-*b*-ethylene oxide) diblock copolymers, J. Polym. Sci. Part B: Polym. Phys. 43 (10) (2005) 1220–1229.
[48] Y. Lin, et al., Self-directed self-assembly of nanoparticle/copolymer mixtures, Nature 434 (7029) (2005) 55–59.
[49] L. Li, et al., Fabrication of robust micro-patterned polymeric films via static breath-figure process and vulcanization, J. Colloid Interface Sci. 354 (2) (2011) 758–764.
[50] C. Ünlü, et al., Developing a facile method for highly luminescent colloidal $CdS \times Se_{1-x}$ ternary nanoalloys, J. Mater. Chem. C 1 (17) (2013) 3026–3034.
[51] F.S. Bates, Polymer-polymer phase behavior, Science 251 (4996) (1991) 898–905.
[52] H. Hasegawa, et al., Bicontinuous microdomain morphology of block copolymers: 1. Tetrapod-network structure of polystyrene-polyisoprene diblock polymers, Macromolecules 20 (7) (1987) 1651–1662.
[53] D.S. Herman, et al., A compositional study of the morphology of 18-armed poly (styrene-isoprene) star block copolymers, Macromolecules 20 (11) (1987) 2940–2942.
[54] S. Foerster, et al., Complex phase behavior of polyisoprene-polystyrene diblock copolymers near the order-disorder transition, Macromolecules 27 (23) (1994) 6922–6935.
[55] A.K. Khandpur, et al., Polyisoprene-polystyrene diblock copolymer phase diagram near the order-disorder transition, Macromolecules 28 (26) (1995) 8796–8806.
[56] M. Matsen, F.S. Bates, Unifying weak-and strong-segregation block copolymer theories, Macromolecules 29 (4) (1996) 1091–1098.
[57] P. Rittigstein, et al., Model polymer nanocomposites provide an understanding of confinement effects in real nanocomposites, Nat. Mater. 6 (4) (2007) 278–282.
[58] M.E. Mackay, et al., General strategies for nanoparticle dispersion, Science 311 (5768) (2006) 1740–1743.
[59] P.F. Green, The structure of chain end-grafted nanoparticle/homopolymer nanocomposites, Soft Matter 7 (18) (2011) 7914–7926.
[60] J. Khan, et al., Polymer crystallization in nanocomposites: spatial reorganization of nanoparticles, Macromolecules 42 (15) (2009) 5741–5744.
[61] V. Pryamitsyn, V. Ganesan, Strong segregation theory of block copolymer-nanoparticle composites, Macromolecules 39 (24) (2006) 8499–8510.
[62] H. Kang, et al., Hierarchical assembly of nanoparticle superstructures from block copolymer-nanoparticle composites, Phys. Rev. Lett. 100 (14) (2008) 148303.